2012

Imaging of poly(α-hydroxy-ester) scaffolds with X-ray phase-contrast microcomputed tomography

Alyssa A. Appel
Illinois Institute of Technology

Jeffery C. Larson
Illinois Institute of Technology

Sami Somo
Illinois Institute of Technology

Zhong Zhong
Brookhaven National Laboratory

Patrick P. Spicer
Rice University

See next page for additional authors

Authors

Alyssa A. Appel, Jeffery C. Larson, Sami Somo, Zhong Zhong, Patrick P. Spicer, Kurtis Kasper, Alfred B. Garson III, Adam M. Zysk, Antonios G. Mikos, Mark A. Anastasio, and Eric M. Brey

TISSUE ENGINEERING: Part C
Volume 18, Number 11, 2012

DOI: 10.1089/ten.tec.2012.0123

Imaging of Poly(α-hydroxy-ester) Scaffolds with X-ray Phase-Contrast Microcomputed Tomography

Alyssa A. Appel, M.S.,[1,2] Jeffery C. Larson, B.S.,[1,2] Sami Somo, B.S.,[1,2] Zhong Zhong, Ph.D.,[3] Patrick P. Spicer, B.S.,[4] F. Kurtis Kasper, Ph.D.,[4] Alfred B. Garson III, Ph.D.,[5] Adam M. Zysk, Ph.D.,[1] Antonios G. Mikos, Ph.D.,[4] Mark A. Anastasio, Ph.D.,[5] and Eric M. Brey, Ph.D.[1,2]

Porous scaffolds based on poly(α-hydroxy-esters) are under investigation in many tissue engineering applications. A biological response to these materials is driven, in part, by their three-dimensional (3D) structure. The ability to evaluate quantitatively the material structure in tissue-engineering applications is important for the continued development of these polymer-based approaches. X-ray imaging techniques based on phase contrast (PC) have shown a tremendous promise for a number of biomedical applications owing to their ability to provide a contrast based on alternative X-ray properties (refraction and scatter) in addition to X-ray absorption. In this research, poly(α-hydroxy-ester) scaffolds were synthesized and imaged by X-ray PC microcomputed tomography. The 3D images depicting the X-ray attenuation and phase-shifting properties were reconstructed from the measurement data. The scaffold structure could be imaged by X-ray PC in both cell culture conditions and within the tissue. The 3D images allowed for quantification of scaffold properties and automatic segmentation of scaffolds from the surrounding hard and soft tissues. These results provide evidence of the significant potential of techniques based on X-ray PC for imaging polymer scaffolds.

Introduction

Tissue engineering involves the generation of a new tissue to replace or repair the failing or damaged tissue.[1] A typical approach involves combinations of biomaterial scaffolds, soluble factors, and cells to promote vascularized tissue formation. Polymeric scaffolds often play a critical role in the success of a tissue engineering therapy, as they provide structural support and mechanical strength, and can directly influence tissue response based on physical, mechanical, and chemical signaling. The physical structure of these scaffolds is critical to their success, and quantitative three-dimensional (3D) imaging tools are needed that enable a more thorough analysis of tissue engineering scaffolds.

Poly(α-hydroxy esters), including poly(lactic-co-glycolic acid) (PLGA) and poly(L-lactic acid) (PLLA), are some of the most widely investigated biomaterials and have been studied in a broad range of tissue engineering applications.[2–5] A variety of techniques are available for generating scaffolds with an interconnected porous structure and tunable degradation kinetics. Success in a particular tissue engineering application requires choosing the appropriate polymer, porous structure, mechanical properties, and the degradation rate of these materials. Degradation of PLGA and PLLA *in vitro* has been extensively studied in an attempt to predict behavior in the body.[6–13] However, tracking 3D tissue invasion and material degradation *in vitro* and *in vivo* without sample alteration is very important for assessing the efficacy of the tissue engineering strategy. Current methods employed in tissue engineering are invasive, require sample destruction, and provide only 2D images. Recently, a multiagency government working group (MultiAgency Tissue Engineering Science Interagency Working Group) identified imaging technologies for a 3D analysis of polymeric scaffolds and engineered tissues as a strategic priority for federal agencies involved in tissue engineering research.[14]

Conventional absorption-based X-ray techniques have been employed to reveal structural details of polymer scaffolds, but only when samples are dried and then imaged in air. Most polymeric scaffolds generate little or no X-ray absorption contrast when in cell culture, bioreactor, or tissue environments. In the past decade, novel X-ray imaging techniques based on phase contrast (PC)[15–17] have shown promise for biomedical applications due to their ability to provide information about tissue structures that only weakly absorb X-rays, but generate contrast based on variations in

[1]Department of Biomedical Engineering, Illinois Institute of Technology, Chicago, Illinois.
[2]Hines Veterans Administration Hospital, Hines, Illinois.
[3]National Synchrotron Light Source, Brookhaven National Laboratory, Upton, New York.
[4]Department of Bioengineering, Rice University, Houston, Texas.
[5]Department of Biomedical Engineering, Washington University in St. Louis, St. Louis, Missouri.

their X-ray refractive index values.[18] Preliminary studies have successfully utilized analyzer-based PC imaging systems for 2D imaging of low-density biomaterials[19,20] in culture conditions; however, 3D computed tomography (CT) has not been investigated.

In this study, we investigated the use of two X-ray PC imaging techniques for imaging porous poly(α-hydroxy-ester) scaffolds. The first technique, an analyzer-based method known as multiple image radiography (MIR), was implemented at a synchrotron imaging facility. The MIR technique produces three separate images that depict the X-ray absorption, refraction, and ultra-small-angle-X-ray-scatter (USAXS) properties of the samples. The second technique, called propagation-based PC imaging, is an in-line holographic method that reveals the locations of discontinuities in an object's X-ray refractive index distribution. This technique was implemented with an X-ray tube source to show the potential for in-lab X-ray PC imaging of engineered tissues. Both techniques were evaluated for imaging polymer scaffolds in cell culture conditions and in a model tissue engineering application.

Background

Four primary implementations of X-ray PC imaging are available: propagation-based PC imaging, X-ray interferometry, differential PC imaging using X-ray gratings, and analyzer-based imaging using crystals. Propagation-based PC imaging is the easiest to implement, since it can achieve PC with a polychromatic beam from a microfocus X-ray tube without using X-ray optical elements. The transmitted X-ray wavefield is allowed to propagate behind the object before its intensity is recorded by a detector. The detector is placed a significant distance downstream from the sample, unlike typical absorption-based X-ray systems, where the detector is placed directly behind the object. The act of free space wavefield propagation in the postsample space induces PC effects into the measured intensity image. This results in an edge enhancement effect at image locations corresponding to the projected tissue interfaces. The object-to-detector distance can be chosen to optimize this edge enhancement while minimizing image blurring due to partial spatial coherence of the X-ray wavefield. Many variations of the technique have been developed by taking images at different detector distances allowing production of either two separate images representing a phase and absorption contrast or a single image that is a combination of phase and absorption effects.[18,21]

Analyzer-based imaging employs a crystal that acts as a filter between the sample and the detector. Based on properties of the analyzer crystal, X-rays travelling at or near the crystal's Bragg angle are selected and ultimately passed on to the intensity detector.[22] MIR is an analyzer-based imaging technique that requires data collection at more than five analyzer crystal angles to generate a rocking curve (Fig. 1). Acquiring images at various locations on the rocking curve allows for separation of the absorption, refraction, and USAXS properties of the object into three distinct images. The absorption image is similar to a conventional radiograph; however, it is free of scatter effects that are usually present in traditional X-ray images and reduces contrast. The refraction image depicts the effect of small beam deflections

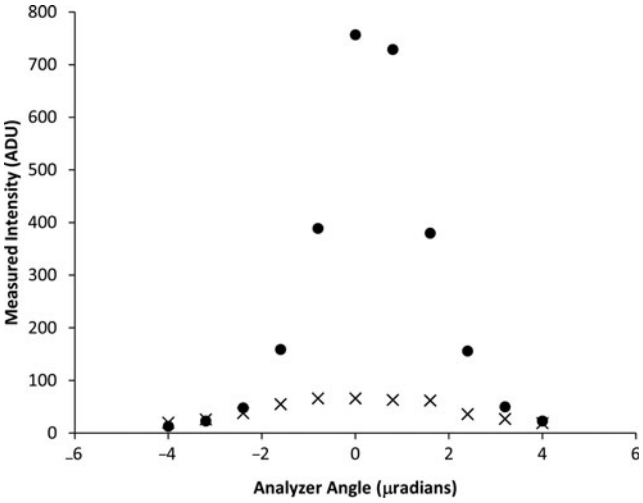

FIG. 1. Example of rocking curves acquired in the absence (●) and presence (x) of a sample.

due to slowly varying refractive index variations in the object and is determined from the shift in the rocking curve distribution when the object is present. The USAXS quantifies angular divergence of the beam caused by the presence of multiple beam refraction from sub-pixel sized scatters and represents broadening of the rocking curve.[23,24] Analyzer-based imaging has mostly been performed using a synchrotron light source, but is being developed for use with X-ray tube sources.[25]

Methods

Preparation of 3D scaffolds

Porous scaffolds were generated using standard salt leaching techniques.[26] PLGA 85:15 (M_w = 50,000–75,000 g/mol) (Sigma-Aldrich) was dissolved in dichloromethane (Sigma-Aldrich). Sieved salt crystals (Fisher Scientific) (300–500 μm) were added to the PLGA solution and the PLGA/salt paste was pressed into a mold and incubated for 6 h to allow the dichloromethane to evaporate. Salt was leached out of the PLGA scaffolds by incubation in deionized water changed every 2–8 h. Scaffolds were placed in phosphate buffer solution (PBS, pH 7) at 37°C for 2, 14, 21, and 29 days for degradation studies.

For the *in vivo* studies, fibrin glue (Tisseel™) (Baxter Healthcare Corp.) was added to nonwoven PLLA fiber mesh scaffolds (Concordia Medical) before implantation in a rat cranial defect as described previously.[27] One group was enriched with platelet-rich plasma and seeded with bone marrow mononuclear cells. Critical-sized, 8-mm-diameter defects were created in the rat calvarium of male Fisher 344 rats (Harlan Bioproducts) (12 weeks old, 225–249 g) and filled with freshly prepared implants and closed. After 12 weeks, animals were euthanized and the implants with surrounding tissues were harvested using a high-speed surgical drill (TPS; Stryker) and the 701 cutting bur.

Synchrotron-based MIR imaging studies

Samples were imaged using an MIR imaging system at Brookhaven National Laboratory (Beamline X15A).[23,28] The X-ray Imager VHR 1:1, CCD (Photonic Science Limited)

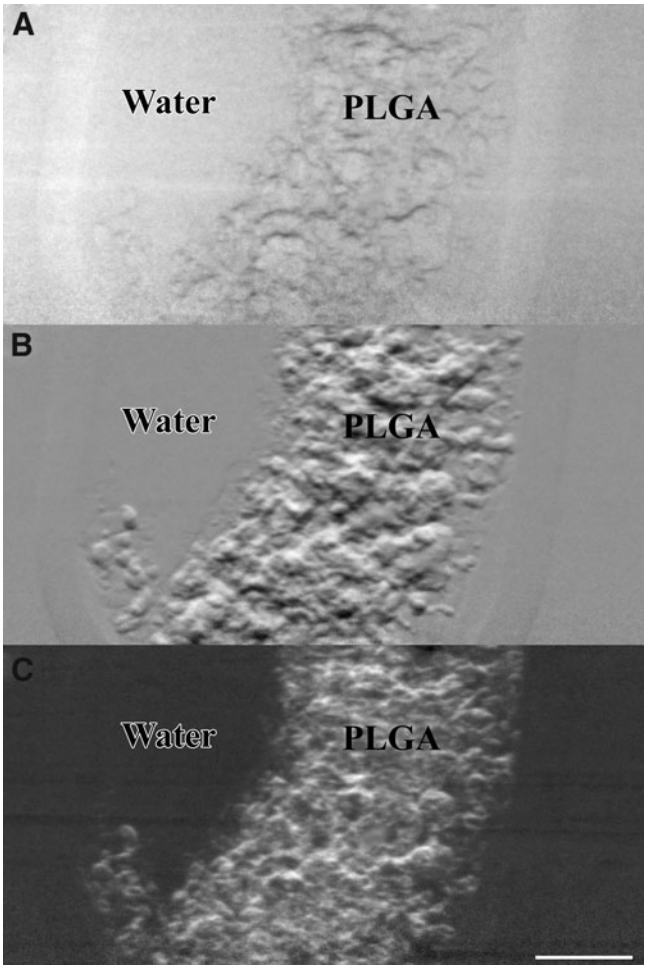

FIG. 2. Calculated MIR projection views: **(A)** Absorption, **(B)** Refraction, and **(C)** USAXS of PLGA scaffold in culture media. Scale bar represents 1 mm. MIR, multiple image radiography; PLGA, poly(lactic-co-glycolic acid); USAXS, ultra-small-angle-X-ray-scatter.

sensor was employed to capture X-rays with a detector pixel size of 9 μm. A monochromated beam of 20 keV and an [333] analyzer crystal reflection were utilized. The measurement data were acquired at 11 analyzer crystal positions, in the presence and absence of the sample, ranging from −4 to +4 μrad to generate a rocking curve (Fig. 1) for each pixel in the detector. Five hundred tomographic intensity measurements were acquired over a 180° angular range for each analyzer-crystal orientation. The acquisition time at each orientation was 1 s. At each tomographic view angle, three parametric MIR images that represent projected absorption (Fig. 2A), refraction (Fig. 2B), and USAXS (Fig. 2C) properties of the sample were computed according to the equations in Table 1.[23] From knowledge of the three MIR images computed at each tomographic view angle, a parallel-beam filtered back-projection algorithm was employed to reconstruct volumetric images of the three MIR properties.[23,28] All image analyses and reconstruction were performed by use of MATLAB R2009b (Mathworks), while V3D (www.vaa3-d.org) was used as the rendering software.

The MIR absorption images of the cranial defects were segmented into three regions of PLLA, bone, and soft tissue using an algorithm created in MATLAB. The bone regions were filled in and then thresholded in the enhanced image. The regions defined as bone were then set to zero to threshold the remaining images to segment the PLLA from the soft tissue.

Benchtop propagation-based PC imaging studies

Benchtop studies of propagation-based PC imaging were conducted at Washington University in St. Louis. This imaging system employed a microfocus X-ray tube with a Tungsten anode (Thermo Kevex PXS10-65W; 7–100 micron spot size, 65W tube power, 45–130 kVp) and a deep cooled high-resolution X-ray camera (Princeton Instruments Quad RO 4096; 15 μm pitch, 16-bit quantization) mounted on a vibration-isolated optical table and housed in a shielded room. The sample and detector were mounted to a long-travel optical rail assembly (Thorlabs XT95SP-1000) for z-axis translation. The sample was positioned by a pair of computer-controlled linear translation stages (Thorlabs LTS150) and a computer-controlled rotation stage (Thorlabs NR360S). Source control and image acquisition were performed via a computer at a remote location outside the shielded room.

The samples were placed 62.3 cm from the source and 106.9 cm from the detector, resulting in a magnification of 2.72. The X-ray tube voltage was set at 55 kVp with a current of 200 μA corresponding to a nominal focal spot size of 13 μm. The system spatial resolution was calculated as 14.7 μm. The exposure time was 39 s.

Benchtop micro-CT

The cranial bone defects were also imaged using a high-resolution SkyScan-1172 micro-CT (μCT) imaging system

Table 1. Equations Used for Computation of Multiple Image Radiography Parametric Images

Normalized rocking curve	$\mathrm{Y}_{m,n}[k] = \frac{y_{m,n}[k]}{\sum_{k=1}^{K} y_{m,n}[k]}$
Intensity measured in the absence of object	$I_0 = \sum_{k=1}^{K} R[k]$
Absorption image	$p_{m,n} = -ln\frac{\sum_{k=1}^{K} y_{m,n}[k]}{I_0}$
Refraction image	$\Delta\theta_{m,n} = \sum_{k=1}^{K}\left(k-\frac{K+1}{2}\right)\mathrm{Y}_{m,n}[k]\Delta - \frac{1}{I_0}\sum_{k=1}^{K}\left(k-\frac{K+1}{2}\right)R[k]\Delta$
USAXS image	$M_{m,n} = \sum_{k=1}^{K}\left[\left(k-\frac{K+1}{2}\right)\Delta - \Delta\theta_{m,n}\right]^2 \mathrm{Y}_{m,n}[k] - \frac{1}{I_0}\sum_{k=1}^{K}\left[\left(k-\frac{K+1}{2}\right)\Delta - \Delta\frac{1}{I_0}\sum_{k=1}^{K}\left(k-\frac{K+1}{2}\right)R[k]\Delta\right]^2 R[k]$

m,n denote pixel location, $y_{m,n}$ denotes measured values in the presence of object, R denotes measured values in the absence of object, k denotes discrete analyzer position, K denotes number of points acquired of rocking curve, Δ denotes the angular spacing of the measured samples.
USAXS, ultra-small-angle-X-ray-scatter.

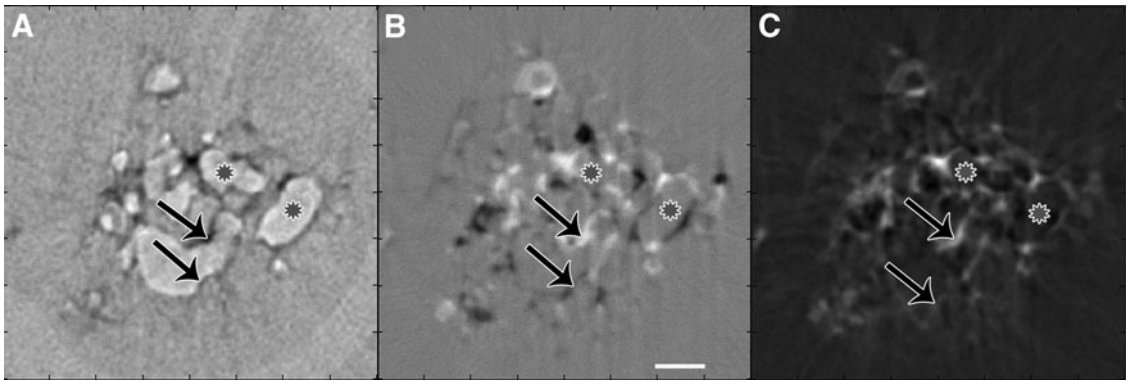

FIG. 3. **(A)** Absorption, **(B)** Refraction, and **(C)** USAXS images of a single CT slice of a PLGA scaffold in culture. Scale bar represents 450 μm. Scaffold walls (arrows) and pores (stars) can be seen in all images. CT, computed tomography.

(SkyScan). The scanner was set to a resolution of 10 μm per pixel. Tube voltage was set at 100 kV and current at 100 μA with a 0.5 mM aluminum filter in place. The resolution was set to high, which created 1280*1024 raw images, and frame averaging was set to four frames per view to increase the signal-to-noise ratio.[29]

Results

Synchrotron-based MIR imaging studies

The MIR PC μCT approach allows reconstruction of volumetric images depicting the X-ray absorption, refraction, and USAXS properties of the samples.[23,28] When examining a single reconstructed slice, all three images allowed visualization of the internal porous structure of PLGA scaffolds in culture conditions (Fig. 3). Pore space, pore walls, and interconnections could be identified in each image. The pores were clear in the absorption image (Fig. 3A), while polymer walls produced a significant contrast in the refraction and USAXS images (Fig. 3B, C). A color-coded volumetric rendering of the three object properties is shown in Figure 4. Porosity and average pore diameter could be quantified from the volumetric renderings (Table 2) and ranged from 80%–91% and 172–226 μm, respectively, over the time period studied.

Cranial defects containing PLLA scaffolds were also imaged using the MIR technique (Fig. 5A–C). Newly formed bone and nondegraded PLLA scaffolds in the defects could be identified in all three MIR images. The MIR absorption represents an ideal absorption-based μCT image that is not degraded by refraction or scatter, which allowed automated segmentation of bone, soft tissue, and PLLA (Fig. 6).

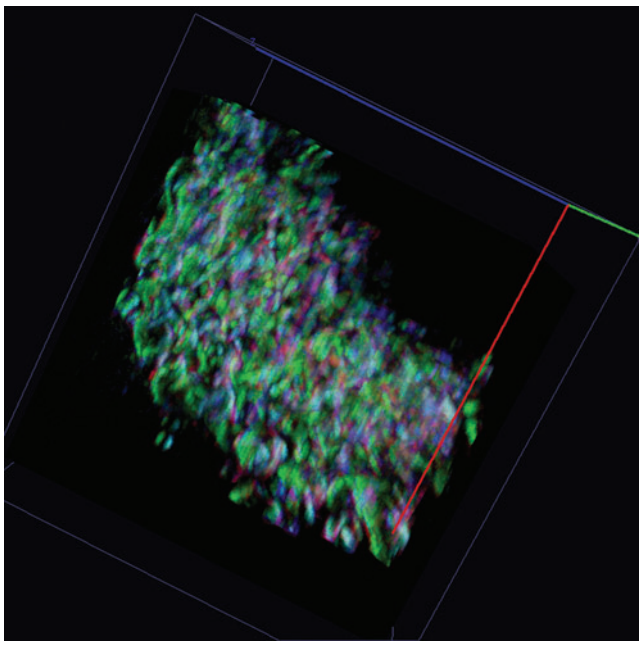

FIG. 4. Three-dimensional volume composite rendering of PLGA scaffold (porosity 80.9%), red represents absorption volume data, green represents refraction volume data, and blue represents USAXS volume data. These composite volumes were thresholded and used to determine porosity of the scaffolds in Table 2. Color images available online at www.liebertpub.com/tec

Benchtop X-ray imaging studies

The cranial defects were also imaged with the benchtop propagation-based PC imaging system as well as a conventional absorption-based μCT system (Fig. 5D, E).[27] The benchtop PC image allowed for the identification of newly formed bone and the remaining PLLA scaffold within the defect, similar to the features detected with the synchrotron-based MIR technique. Fiber structures within the defect could be identified in the PC image (Fig. 5F). The conventional μCT system only revealed newly formed bone within the defect without any contrast from the soft tissue or biomaterial.

Discussion

The fields of tissue engineering and regenerative medicine are in critical need of techniques that allow quantitative 3D

Table 2. Scaffold Properties Measured from Multiple Image Radiography Volume Data

Days	*Porosity*	*Average pore diameter (μm)*
2	80.9%	199.1 ± 47.4
14	86.1%	185.8 ± 44.7
21	91.4%	225.8 ± 38.1
29	86.6%	172.8 ± 47.8

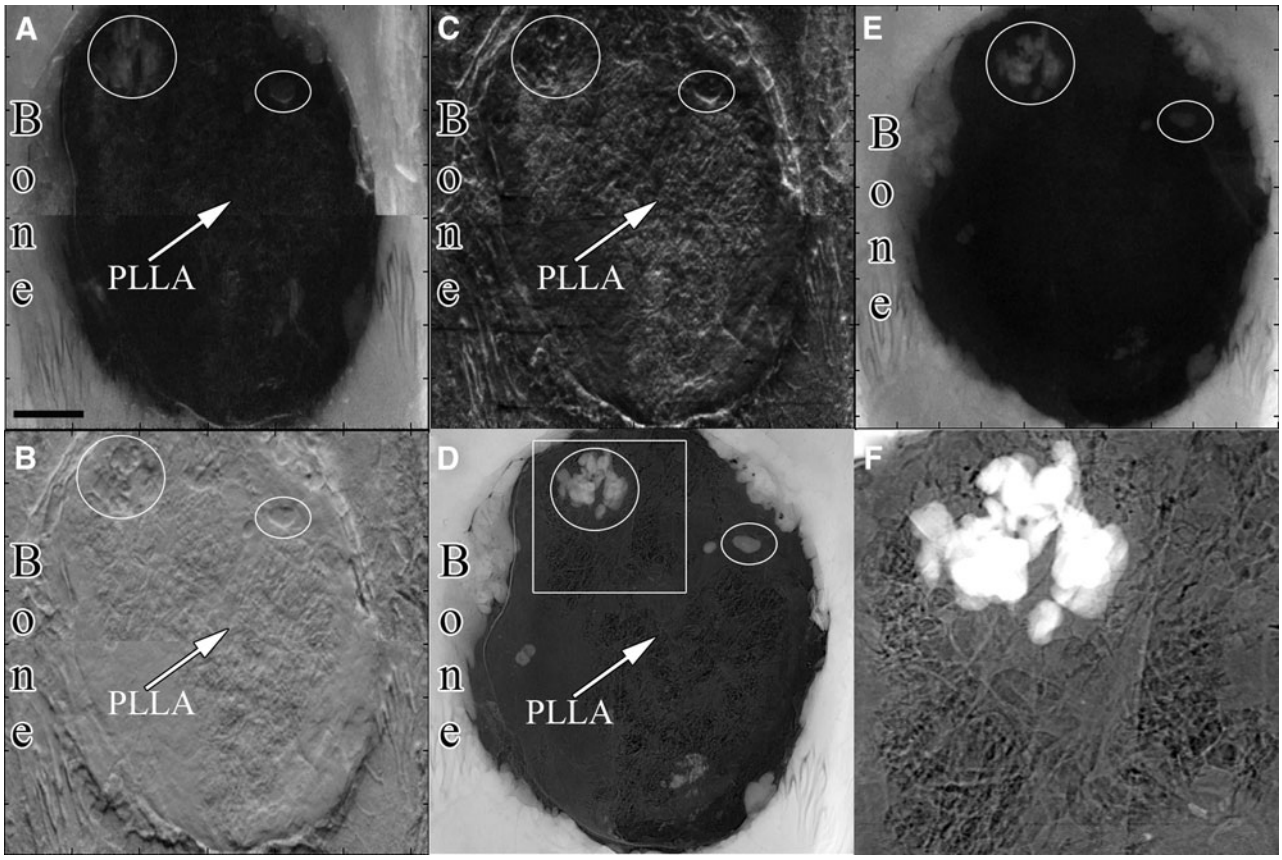

FIG. 5. X-ray images of the cranial defect sample. Synchrotron MIR imaging produces **(A)** Absorption, **(B)** Refraction, and **(C)** USAXS images. **(D)** The benchtop propagation-based PC image produces a single image that is a combination of phase and absorption effects and **(E)** the conventional mCT, which is based on absorption contrast alone. Newly formed bone is seen in images (circles), while the PLLA scaffold (arrow) is visible in the PC images [three MIR images **(A–C)** and the benchtop image **(D)**], but not the mCT **(E)**. **(F)** The magnified region of newly formed bone and PLLA fibers from inset (box) in region of **(D)**. Scale bar represents 1.8 mm. PC, phase contrast; microCT, microcomputed tomography; PLLA, poly(L-lactic acid).

evaluation of the polymer scaffold structure.[14] In this study, we have shown that X-ray PC imaging techniques allowed for visualization of polymer scaffolds in culture media and a model engineered tissue. Previously, scaffolds required dry conditions to see the internal structure with traditional X-ray techniques. However, X-ray PC imaging allows for visualization of the scaffold structure without sample drying or addition of exogenous contrast agents.

X-ray PC imaging enabled visualization of important scaffold features in both *in vitro* culture conditions and *ex vivo* tissue sample imaging. PLGA scaffolds in cell culture conditions generated contrast in all three MIR images,

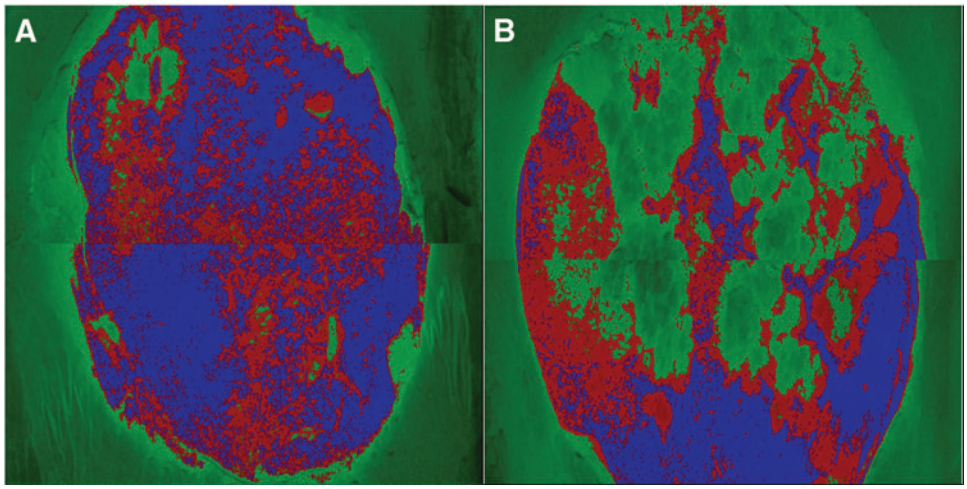

FIG. 6. Segmented MIR absorption images indicating separate identification of regions of bone (green), PLLA (red), and soft tissue (blue). Samples show **(A)** low bone formation in the PLLA/Fibrin scaffold alone and **(B)** enhanced bone formation in the presence of the PLLA/Fibrin scaffold enriched with platelet-rich plasma and bone marrow mononuclear cells. Color images available online at www.liebertpub.com/tec

allowing 3D imaging of the pore volume and scaffold walls. In *ex vivo* imaging, X-ray PC allowed for the identification of newly formed bone within the cranial defect and allowed identification of the residual polymer scaffold. The scaffold was invisible in conventional μCT images. MIR absorption images allowed for segmentation of defect into regions of bone, PLLA, and soft tissue. This is very important for assessing the success of the tissue engineering approach and can be used to quantify new bone formation and perhaps PLLA degradation if multiple time points had been imaged. The benchtop imaging system also allowed for easy differentiation of PLLA from bone within a single image.

In addition to imaging scaffold features when using X-ray PC, important properties could be quantified. Using MIR μCT, the internal porous structure could be reconstructed to measure pore size and porosity. The porosity calculated in this study from MIR volumes is consistent with other PLGA scaffolds generated with similarly sized porogens. Porous PLGA scaffolds prepared using sieved salt crystal of 300–500 μm result in pore diameters between 100 and 250 microns.[10] Evaporation of dichloromethane reduces scaffold volume resulting in pore sizes less than the initial salt size. In this study, porosity did not vary over the time frame investigated. This is not surprising, as previous studies with PLGA of similar composition and structure did not find significant morphological changes or weight loss over 4 weeks of degradation.[8,10,30–32] The degradation time scale for this copolymer ratio and molecular weight should be greater than one month.[33] Overall, MIR μCT imaging allowed for the visualization of PLGA scaffolds and provided the ability to quantify important scaffold characteristics under culture conditions.

In this study, tissue samples were imaged with MIR utilizing a synchrotron light source, a benchtop propagation-based PC imaging and a commercially-available μCT system allowing direct comparisons of these imaging methods. Both PC imaging techniques (MIR and propagation based) allowed visualization of polymer scaffolds and soft tissue within the tissue implant, which was not possible with conventional μCT. The MIR results provide evidence that nontraditional X-ray contrast mechanisms are produced in engineered tissues and can be imaged with X-ray PC. However, the use of a synchrotron light source limits the broad applicability of this method. The propagation-based system utilized a microfocus X-ray tube, but was able to identify similar sample features to the synchrotron-based system. This is the first study where engineered tissue was successfully imaged with a benchtop PC imaging system and provides strong support for further development and testing of X-ray PC for imaging biomaterials and engineered tissues.

These results show that X-ray PC imaging can be used to visualize polyester scaffolds in tissue engineering applications. The polyester scaffolds exhibit different X-ray contrast mechanisms from porous hydrogels in the MIR images.[19] The μCT approach allowed 3D imaging and quantification of the scaffold structure. Poly(α-hydroxy esters) scaffolds could also be identified in tissue samples and could be distinguished from hard and soft tissues with both the synchrotron and microfocus X-ray tube PC imaging techniques. This work provides additional evidence for the strong potential of X-ray PC for imaging biomaterials used in tissue engineering.

Acknowledgments

The research has been supported by the Veterans Administration, the National Science Foundation (0854430, 0731201, and 0546113) and the National Institute of Health (R01EB009715 and F32CA136102).

Disclosure Statement

No competing financial interests exist.

References

1. Brey, E.M., and Patrick, Jr., C.W. Engineering applied to reconstructive surgery. IEEE Eng Med Biol **19,** 122, 2000.
2. Baker, S.C., Rohman, G., Southgate, J., and Cameron, N.R. The relationship between the mechanical properties and cell behaviour on PLGA and PCL scaffolds for bladder tissue engineering. Biomaterials **30,** 1321, 2009.
3. Lavik, E.B., Klassen, H., Warfvinge, K., Langer, R., and Young, M.J. Fabrication of degradable polymer scaffolds to direct the integration and differentiation of retinal progenitors. Biomaterials **26,** 3187, 2005.
4. Tanaka, Y., Yamaoka, H., Nishizawa, S., Nagata, S., Ogasawara, T., Asawa, Y., Fujihara, Y., Takato, T., and Hoshi, K. The optimization of porous polymeric scaffolds for chondrocyte/atelocollagen based tissue-engineered cartilage. Biomaterials **31,** 4506, 2010.
5. Xiong, Y., Zeng, Y.-S., Zeng, C.-G., Du, B.-L., He, L.-M., Quan, D.-P., Zhang, W., Wang, J.-M., Wu, J.-L., Li, Y., and Li, J. Synaptic transmission of neural stem cells seeded in 3-dimensional PLGA scaffolds. Biomaterials **30,** 3711, 2009.
6. Cao, Y., Mitchell, G., Messina, A., Price, L., Thompson, E., Penington, A., Morrison, W., O'connor, A., Stevens, G., and Cooper-White, J. The influence of architecture on degradation and tissue ingrowth into three-dimensional poly(lactic-co-glycolic acid) scaffolds *in vitro* and *in vivo*. Biomaterials **27,** 2854, 2006.
7. Loo, S.C., Ooi, C.P., and Boey, Y.C. Influence of electron-beam radiation on the hydrolytic degradation behaviour of poly(lactide-co-glycolide) (PLGA). Biomaterials **26,** 3809, 2005.
8. Dorati, R., Colonna, C., Genta, I., Modena, T., and Conti, B. Effect of porogen on the physico-chemical properties and degradation performance of PLGA scaffolds. Polym Degrad Stabil **95,** 694, 2010.
9. Jeon, O., Song, S.J., Kang, S.-W., Putnam, A.J., and Kim, B.-S. Enhancement of ectopic bone formation by bone morphogenetic protein-2 released from a heparin-conjugated poly(l-lactic-co-glycolic acid) scaffold. Biomaterials **28,** 2763, 2007.
10. Lee, S.J., Lim, G.J., Lee, J.-W., Atala, A., and Yoo, J.J. *In vitro* evaluation of a poly(lactide-co-glycolide)–collagen composite scaffold for bone regeneration. Biomaterials **27,** 3466, 2006.
11. Orava, E., Korventausta, J., Rosenberg, M., Jokinen, M., and Rosling, A. *In vitro* degradation of porous poly(dl-lactide-co-glycolide) (PLGA)/bioactive glass composite foams with a polar structure. Polym Degrad Stabil **92,** 14, 2007.
12. Sung, H.-J., Meredith, C., Johnson, C., and Galis, Z.S. The effect of scaffold degradation rate on three-dimensional cell growth and angiogenesis. Biomaterials **25,** 5735, 2004.

13. Yang, F., Cui, W., Xiong, Z., Liu, L., Bei, J., and Wang, S. Poly(l,l-lactide-co-glycolide)/tricalcium phosphate composite scaffold and its various changes during degradation *in vitro*. Polym Degrad Stabil **91,** 3065, 2006.
14. Multi-Agency Tissue Engineering Science A Foundation for the Future. Advancing Tissue Science and Engineering: A Multi-Agency Strategic Plan. June 2007. www.tissueengineering.gov/advancing_tissue_science_&_engineering.pdf (accessed January 2012).
15. Laperle, C.M., Wintermeyer, P., Wands, J.R., Shi, D., Anastasio, M.A., Li, X., Ahr, B., Diebold, G.J., and Rose-Petruck, C. Propagation based differential phase contrast imaging and tomography of murine tissue with a laser plasma x-ray source. Appl Phys Lett **91,** 173901, 2007.
16. Mayo, S.C., Davis, T.J., Gureyev, T.E., Miller, P.R., Paganin, D., Pogany, A., Stevenson, A.W., and Wilkins, S.W. X-ray phase-contrast microscopy and microtomography. Opt Expr **11,** 2289, 2003.
17. Lewis, R.A. Medical phase contrast x-ray imaging: current status and future prospects. Phys Med Biol **49,** 3573, 2004.
18. Appel, A., Anastasio, M.A., and Brey, E.M. Potential for imaging engineered tissues with X-ray phase contrast. Tissue Eng Part B Rev **17,** 321, 2011.
19. Brey, E.M., Appel, A., Chiu, Y.C., Zhong, Z., Cheng, M.H., Engel, H., and Anastasio, M.A. X-ray imaging of poly(ethylene glycol) hydrogels without contrast agents. Tissue Eng Part C Methods **16,** 1597, 2010.
20. Zhu, N., Chapman, D., Cooper, D., Schreyer, D.J., and Chen, X. X-Ray Diffraction enhanced imaging as a novel method tovisualize low-density scaffolds in soft tissue engineering. Tissue Eng Part C Methods **17,** 1, 2011.
21. Cloetens, P., Ludwig, W., Baruchel, J., Van Dyck, D., Van Landuyt, J., Guigay, J.P., and Schlenker, M. Holotomography: quantitative phase tomography with micrometer resolution using hard synchrotron radiation x rays. Appl Phys Lett **75,** 2912, 1999.
22. Chapman, D., Thomlinson, W., Johnston, R.E., Washburn, D., Pisano, E., Gmur, N., Zhong, Z., Menk, R., Arfelli, F., and Sayers, D. Diffraction enhanced x-ray imaging. Phys Med Biol **42,** 2015, 1997.
23. Brankov, J.G., Wernick, M.N., Yang, Y., Li, J., Muehleman, C., Zhong, Z., and Anastasio, M.A. A computed tomography implementation of multiple-image radiography. Med Phys **33,** 278, 2006.
24. Wernick, M.N., Wirjadi, O., Chapman, D., Zhong, Z., Galatsanos, N.P., Yang, Y., Brankov, J.G., Oltulu, O., Anastasio, M.A., and Muehleman, C. Multiple-image radiography. Phys Med Biol **48,** 3875, 2003.
25. Nesch, I., Fogarty, D.P., Tzvetkov, T., Reinhart, B., Walus, A.C., Khelashvili, G., Muehleman, C., and Chapman, D. The design and application of an in-laboratory diffraction-enhanced x-ray imaging instrument. Rev Sci Instrum **80,** 093702, 2009.
26. Yang, Y., Zhao, J., Zhao, Y., Wen, L., Yuan, X., and Fan, Y. Formation of porous PLGA scaffolds by a combining method of thermally induced phase separation and porogen leaching. J Appl Polym Sci **109,** 1232, 2008.
27. Kretlow, J.D., Spicer, P.P., Jansen, J.A., Vacanti, C.A., Kasper, F.K., and Mikos, A.G. Uncultured marrow mononuclear cells delivered within fibrin glue hydrogels to porous scaffolds enhance bone regeneration within critical-sized rat cranial defects. Tissue Eng Part A **16,** 3555, 2010.
28. Chou, C.-Y., Anastasio, M.A., Brankov, J.G., Wernick, M.N., Brey, E.M., Connor, D.M., and Zhong, Z. An extended diffraction-enhanced imaging method for implementing multiple-image radiography. Phys Med Biol **52,** 1923, 2007.
29. Young, S., Patel, Z.S., Kretlow, J.D., Murphy, M.B., Mountziaris, P.M., Baggett, L.S., Ueda, H., Tabata, Y., Jansen, J.A., Wong, M., and Mikos, A.G. Dose effect of dual delivery of vascular endothelial growth factor and bone morphogenetic protein-2 on bone regeneration in a rat critical-size defect model. Tissue Eng Part A **15,** 2347, 2009.
30. Lu, L., Peter, S.J., Lyman, M.D., Lai, H.-L., Leite, S.M., Tamada, J.A., Uyama, S., Vacanti, J.P., Langer, R., and Mikos, A.G. *In vitro* and *in vivo* degradation of porous poly(DL-lactic-co-glycolic acid) foams. Biomaterials **21,** 1837, 2000.
31. Wu, L., and Ding, J. *In vitro* degradation of three-dimensional porous poly(d,l-lactide-co-glycolide) scaffolds for tissue engineering. Biomaterials **25,** 5821, 2004.
32. Wu, L., Jing, D., and Ding, J. A "room-temperature" injection molding/particulate leaching approach for fabrication of biodegradable three-dimensional porous scaffolds. Biomaterials **27,** 185, 2006.
33. Lee, S.-H., and Shin, H. Matrices and scaffolds for delivery of bioactive molecules in bone and cartilage tissue engineering. Adv Drug Deliv Rev **59,** 339, 2007.

Address correspondence to:
Eric M. Brey, Ph.D.
Department of Biomedical Engineering
Illinois Institute of Technology
3255 South Dearborn St.
Chicago, IL 60616

E-mail: brey@iit.edu

Received: February 27, 2012
Accepted: May 2, 2012
Online Publication Date: July 2, 2012